



Thrombopoietic agents enhance bone healing in mice, rats, and pigs

Paul J. Childress^{1,2}, Jeffery J. Nielsen^{3,4}, Thomas B. Bemenderfer¹, Ushashi C. Dadwal^{1,2}, Nabarun Chakraborty⁵, Jonathan S. Harris¹, Monique Bethel¹, Marta B. Alvarez^{1,2}, Aamir Tucker¹, Alexander R. Wessel¹, Patrick D. Millikan¹, Jonathan H. Wilhite¹, Andrew Engle¹, Alexander Brinker¹ , Jeffrey D. Rytlewski¹, David C. Scofield¹, Kaitlyn S. Griffin¹, W. Christopher Shelley⁶, Kelli J. Manikowski⁷, Krista L. Jackson⁷, Stacy-Ann Miller⁵, Ying-Hua Cheng¹, Joydeep Ghosh⁸, Patrick L. Mulcrone^{1,2}, Edward F. Srouf^{6,8}, Mervin C. Yoder⁶, Roman M. Natoli¹, Karl D. Shively¹, Aarti Gautam⁵, Rasha Hammamieh⁵, Stewart A. Low⁴, Philip S. Low^{3,4}, Todd O. McKinley¹, Jeffrey O. Anglen¹, Jonathan W. Lowery⁷, Tien-Min G. Chu⁹, Melissa A. Kacena^{1,2,*} 

¹Department of Orthopaedic Surgery, Indiana University School of Medicine, Indianapolis, IN, 46202, United States

²Richard L. Roudebush VA Medical Center, Indianapolis, IN, 46202, United States

³Department of Medicinal Chemistry and Molecular Pharmacology, Purdue University, West Lafayette, IN, 47907, United States

⁴Department of Chemistry, Purdue University, West Lafayette, IN, 47907, United States

⁵Medical Readiness Systems Biology, Walter Reed Army Institute of Research, Silver Spring, MD, 20910, United States

⁶Department of Pediatrics, Indiana University School of Medicine, Indianapolis, IN, 46202, United States

⁷Division of Biomedical Science, Marian University College of Osteopathic Medicine, Indianapolis, IN, 46222, United States

⁸Department of Medicine, Indiana University School of Medicine, Indianapolis, IN, 46202, United States

⁹Department of Biomedical and Applied Sciences, Indiana University School of Dentistry, Indianapolis, IN, 46202, United States

*Corresponding author: Melissa A. Kacena, Indiana Center for Musculoskeletal Health, Chancellor's Professor and Vice Chair for Research, Edward H. and Yvonne J. Boseker Professor of Orthopaedics, Indiana University School of Medicine, 635 Barnhill Drive, MS549, Indianapolis, IN 46202, United States and Research Career Scientist, Rehabilitation Research & Development Service, Richard L. Roudebush VA Medical Center, Indianapolis, IN, 46202, United States (mkacena@iu.edu)

Abstract

Achieving bone union remains a significant clinical dilemma. The use of osteoinductive agents, specifically bone morphogenetic proteins (BMPs), has gained wide attention. However, multiple side effects, including increased incidence of cancer, have renewed interest in investigating alternatives that provide safer, yet effective bone regeneration. Here we demonstrate the robust bone healing capabilities of the main megakaryocyte (MK) growth factor, thrombopoietin (TPO), and second-generation TPO agents using multiple animal models, including mice, rats, and pigs. This bone healing activity is shown in two fracture models (critical-sized defect [CSD] and closed fracture) and with local or systemic administration. Our transcriptomic analyses, cellular studies, and protein arrays demonstrate that TPO enhances multiple cellular processes important to fracture healing, particularly angiogenesis, which is required for bone union. Finally, the therapeutic potential of thrombopoietic agents is high since they are used in the clinic for other indications (eg, thrombocytopenia) with established safety profiles and act upon a narrowly defined population of cells.

Keywords: thrombopoietin, bone healing, fracture, bone repair, bone regeneration

Lay Summary

Fractures that fail to heal can be devastating injuries. Treatment options are limited and center on stimulating bone growth. However, this treatment does not fully stimulate the many cell types in natural healing. Megakaryocytes (MKs) are “first responders” to injury and begin the healing process. We have investigated delivering thrombopoietic agents, which stimulate MK growth, directly to fractures incapable of healing. We found these agents can aid in healing such fractures in mice, rats, and pigs. Thrombopoietic agents are currently Food and Drug Administration (FDA)-approved for certain blood conditions. Our work suggests repurposing these agents to help heal fractures that may otherwise never heal.

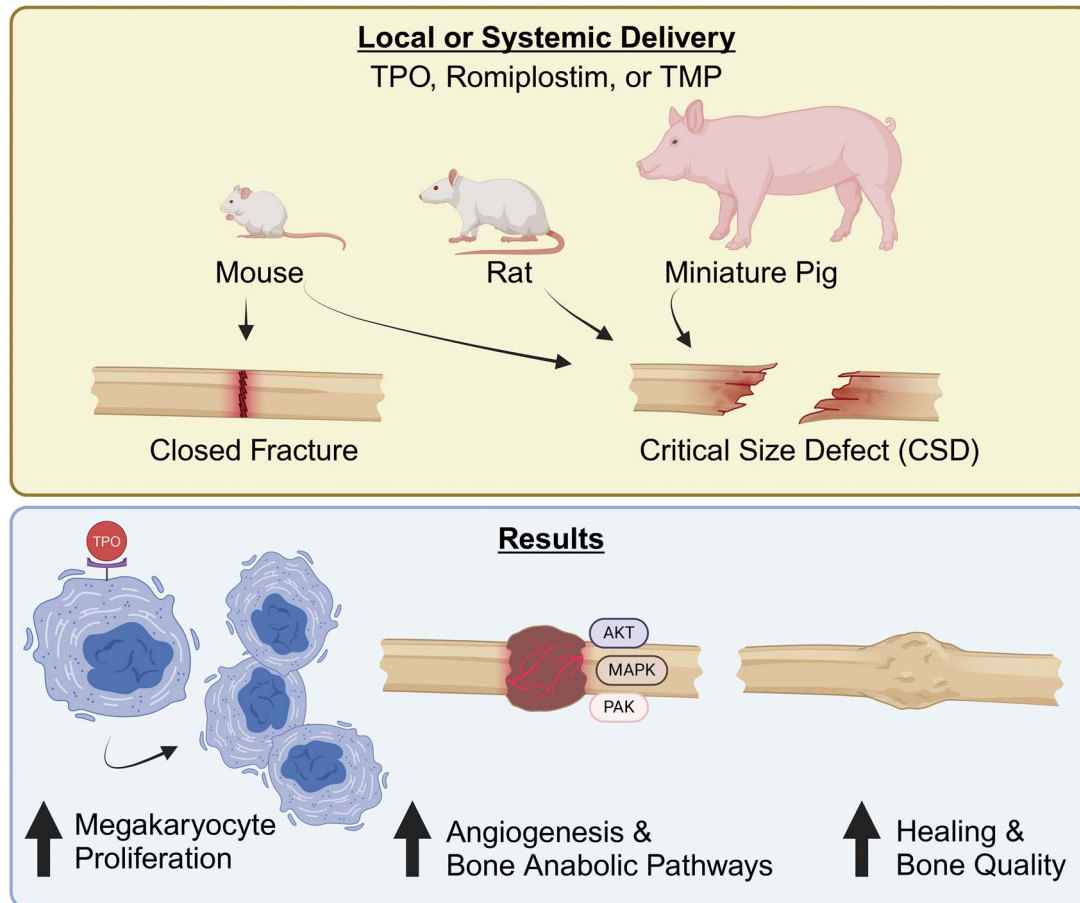
Received: April 25, 2023. Revised: October 15, 2024. Accepted: November 19, 2024

© The Author(s) 2024. Published by Oxford University Press on behalf of the American Society for Bone and Mineral Research.

This is an Open Access article distributed under the terms of the Creative Commons Attribution Non-Commercial License

(<https://creativecommons.org/licenses/by-nc/4.0/>), which permits non-commercial re-use, distribution, and reproduction in any medium, provided the original work is properly cited. For commercial re-use, please contact journals.permissions@oup.com

Graphical Abstract



Introduction

Fractures and skeletal defects are wounds that can heal without significant scarring. The initial wounding event stimulates platelet-forming megakaryocytes (MKs) to establish hemostasis, quickly followed by innate immune cell recruitment, including neutrophils and M1-type macrophages in the local area.¹ The cellular recruitment, molecular cues, and eventual anatomic remodeling of an intact skeletal structure are extremely complex.^{2,3} This complexity gives rise to many opportunities to forestall healing, such as dysregulation of the inflammatory response⁴ and insufficient vascular invasion.⁵ Indeed, the incidence of delayed or failed healing in skeletal defects has been persistently high despite advances in surgical methodology and improved implants.⁶

Many pharmacological approaches have been examined for enhancing fracture healing, including local or systemic administration of bone anabolic agents, such as various cytokines (eg, BMPs, PDGF, VEGF), parathyroid hormone, neutralizing antibodies (eg, α -SOST, α -DKK antibodies), and minimally manipulated patient-derived platelet-rich plasma. To varying degrees, these agents can successfully stimulate bone growth in animal models, but to date only bone morphogenetic proteins (BMPs) and platelet-derived growth factor (PDGF) have been approved by the Food and Drug Administration (FDA) for fracture healing indications, with much of the clinical use being off-label. Unfortunately, since BMP-2 received approval,

it has been associated with significant side-effects, including heterotopic ossification and an increased risk of developing cancer.⁷

Interestingly, multiple mouse genetic models have demonstrated that increases in bone marrow MKs are associated with a high bone mass phenotype and that MKs stimulate osteoblast proliferation and bone formation.⁸⁻¹⁴ These observations raise the possibility that increasing MKs locally at the fracture site could enhance bone healing. Thrombopoietin (TPO), the main MK growth factor, works through its cognate receptor, Mpl. TPO is exquisitely selective for binding to Mpl, having little cross-reactivity with receptors for structurally related hematopoietic growth factors (eg, erythropoietin or EPO and its receptor EPOR).^{15,16} Additionally, the tissue distribution of Mpl expression is restricted compared to several other receptors for agents used to enhance bone healing. [Figure S1](#) shows gene expression levels in several tissues for Mpl, BMPR1a, Flt1 (VEGFR1), PDGFR β , TGF β 1, and PTHR1 compiled from the Human Protein Atlas.¹⁷ Mpl is not broadly expressed in bulk tissue preparations compared to these other receptors, which is consistent with previous reports.¹⁸ Combined, the specificity for TPO with Mpl and limited receptor expression are consistent with the profile of an attractive therapeutic target. Indeed, a TPO-mimetic and small-molecule agonist of Mpl are FDA-approved agents to treat idiopathic thrombocytopenic purpura with established

safety profiles.^{19,20} Thus, expanding the therapeutic potential of this axis to include bone healing is an intriguing possibility.

Materials and methods

Scaffolds

Poly(propylene) fumarate/tricalcium phosphate scaffolds were synthesized by utilizing a 3D-printed mold in various sizes as described previously.²¹ Photos of rat and mouse scaffolds as well as rat scaffold dimensions are detailed in [Figure S2](#). Specifically, the scaffolds for rats were manufactured with a 4 mm outer diameter, a 2 mm inner diameter, and a 5 mm height (length). Scaffolds used in mice were similarly manufactured as for rats, except the outer diameter was 2 mm, the inner diameter was 1 mm, and 4 mm in height (length). Four side-holes (0.4 mm diameter) were contained within these scaffolds to allow the drug to access the bone marrow environment. Larger scaffolds for pigs were also synthesized as above, with the addition of 2 mm holes through the scaffold shell to allow communication between marrow space and periosteal space. Holes were offset from the center and separated from each other by 2 mm (see [Figure S3](#)). The outer diameter was 16 mm, the inner diameter was 9 mm, and 25 mm in height (length).

Synthesis of TMP

Dimerized TPO mimetic peptides (TMP) have been demonstrated to have essentially the same activity as the full TPO protein,¹⁵ and AF13948, the dimer of AF12505, has been demonstrated to have particularly high potency and stability and was synthesized to be used as a systemically administered drug. AF13948 (TMP) was synthesized according to standard Fmoc solid-phase peptide synthesis procedures. Briefly, TMP was synthesized in a solid-phase peptide synthesis vial under a stream of argon. 2-chlorotrityl resin (0.6 mmol/g) was loaded at 0.6 mmol/g with N α ,N ϵ -di-Fmoc-L-lysine for 60 min in dichloromethane (DCM) and diisopropylethylamine. The resin was then capped with four washes of HPLC-grade MeOH, followed by three washes with DCM and N-dimethylformamide (DMF), consecutively. After each amino acid coupling reaction, 9-fluorenylmethoxycarbonyl (Fmoc) groups were removed by two 10-min incubations with 20% (v/v) piperidine in DMF. The resin was then washed twice with DMF prior to the addition of the next amino acid. Each amino acid was reacted in a 3-fold excess with 2-(1H-benzotriazol-1-yl)-1,1,3,3-tetramethyluronium hexafluorophosphate (HBTU)/N-methylmorpholine (NMM) for 30 min. Followed by a double coupling with 3-fold excess benzotriazol-1-yl-oxytripyrrolidinophosphonium hexafluorophosphate (PyBOP)/N-methylmorpholine (NMM) for 30 min. All amino acids were added according to the conditions above. Thereafter, the following peptide sequence was added onto the peptide using the solid phase procedures listed above using the AAPTEC FOCUS XC automated peptide synthesizer: Ile-Glu-Gly-Pro-Thr-Leu-Arg-Gln-Npa-Leu-Ala-Ala-Arg-Sar. Upon completion of the synthesis, the terminal Fmoc was removed using the same conditions as listed above, and then the resin was washed three times with DMF and then three times with DCM and then twice with methanol and then dried with argon gas. The dried resin with the peptide was cleaved using 95:2.5:2.5 trifluoroacetic acid:water:triisopropylsilane for 2 hr. The peptide was then

precipitated from the cleavage solution using 10 times the volume of cold diethyl ether. The solution was spun at 2000 rcf for 5 min and then decanted. The pellet was then desiccated and submitted to LCMS for confirmation of synthesis. The crude peptide was dissolved in a mixture of DMF and water and purified via reverse phase preparatory high-performance liquid chromatography. A C-18 column with a 0%-50% ammonium acetate: acetonitrile mobile phase for 40 min was used to purify the TMP. The fraction that contained only pure TMP as assessed by LCMS was lyophilized and stored as a lyophilized powder at -20°C .

Animals and animal surgeries

All animals used in these studies were purchased from approved vendors and were free of known pathogens. Long Evans rats were purchased from Charles River (Malvern, PA), C57BL/6J mice were purchased from Jackson Laboratories (Bar Harbor, ME, RRID:IMSR_JAX:000664), ND4 Swiss Webster mice were purchased from Envigo (Indianapolis, IN), and Yucatán miniature pigs were purchased from Sinclair Bio Resources (Auxvasse, MO). The rodent colonies at both institutions were tested quarterly for pathogens using indirect sentinel exposure. The animal facilities were maintained at $22 \pm 2^{\circ}\text{C}$, and 30%-70% relative humidity. All rodents had ad libitum access to water and Teklad Rodent Diet (Envigo 2018SX) at both Indiana University and Purdue University. Miniature pigs were provided Purina Lab Diet (#5081 or #5084, Orchard Country Store) according to large animal veterinarian recommendations. Mice were housed 5 animals per cage, rats were housed 2 per cage, and Yucatán miniature pigs were individually housed in accordance with IACUC regulations.

Rodent critical-sized defect (CSD) surgeries were performed to induce a femoral segmental bone defect ([Figure S2](#)), as previously described^{21,22}; pig surgeries were performed to induce a tibial segmental bone defect ([Figure S3](#)) as previously described.²³⁻²⁵ All CSD animal experiments were performed in accordance with protocols approved by Indiana University's Institutional Animal Care and Use Committee (IACUC). Closed fracture mouse studies were performed in accordance with protocols approved by Purdue University's IACUC as previously described.²⁶ [Figures 1H, 2E and F, 3I, and 4E](#) illustrate the experimental timeline for each of the animal studies completed in chronological order, starting with our original pilot study with rats, followed by our mouse studies, and ending with our in vivo pig study. We note the number of animals at the beginning of the study, the number of animals that made it to the terminal time point, how many specimens were included in outcome measures, and account for any excluded samples during the studies. Detailed methods for each of the animal surgeries have been previously published,²¹⁻²⁶ but are also contained within the Supplementary Information. Briefly, for the Rat CSD study, 10 adult male Long Evans rats weighting 450-500 g were used. For the mouse CSD studies, 10-wk-old male C57BL/6J mice were used; 15 for the studies in which dicalcium phosphate dihydrate (DCPD) cement was used to deliver drugs, and 37 for the studies in which collagen sponges were used to deliver drugs. In the closed-fracture mouse study, 23 female Swiss Webster mice at 12-wk of age were used. For rodents, cages of animals were randomly assigned into treatment groups. Finally, 24 male Yucatán miniature pigs at 20 mo of age were used for the large-animal CSD

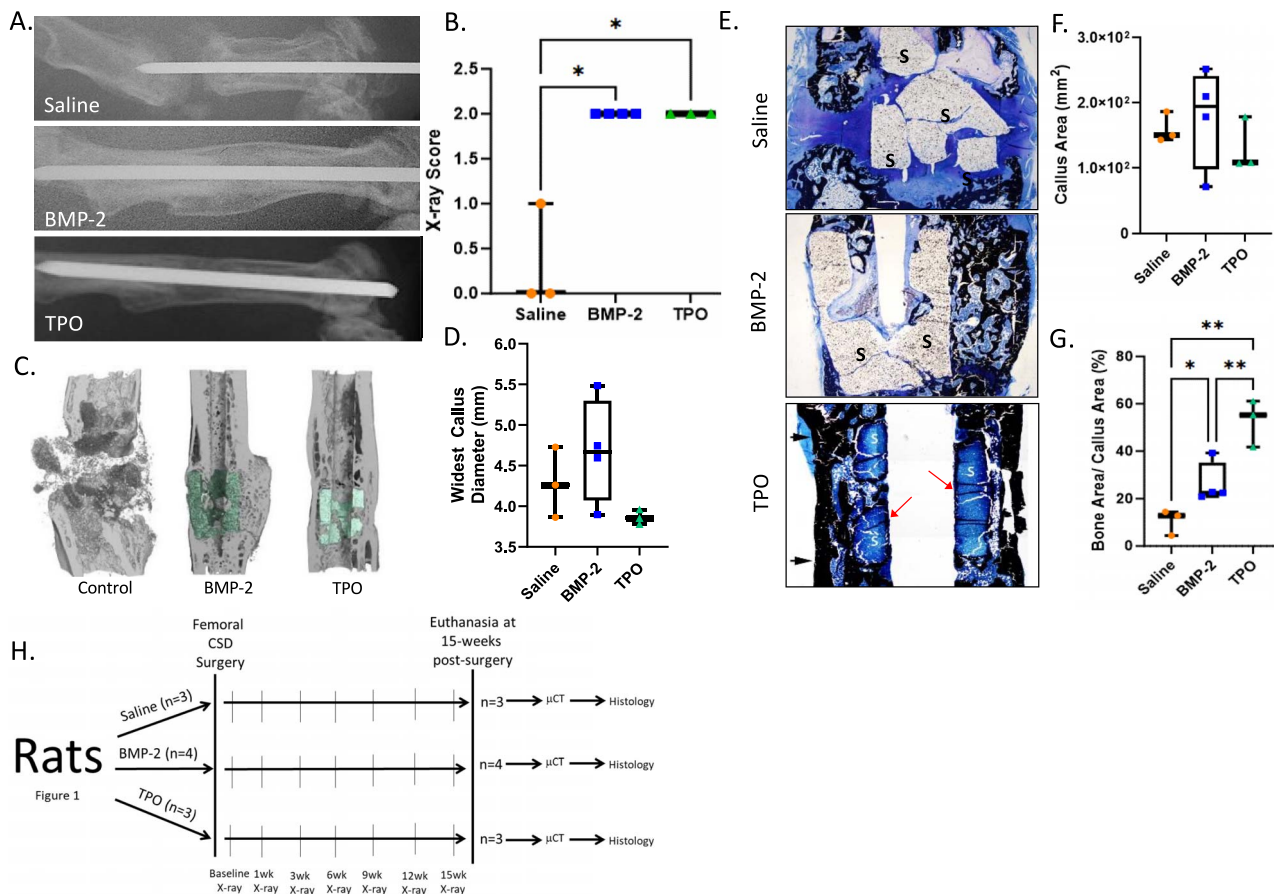


Figure 1. TPO promotes bone healing in a rat CSD model. Male Long Evans rats (450–500 g) underwent CSD surgeries for a pilot study. (A) Representative X-rays taken at 15-wk post-surgery with control (saline, $n = 3$), BMP-2 (10 μg , $n = 3$), or TPO (10 μg , $n = 4$) scaffolds. DCPD cement was used to carry the drugs. (B) Bridging X-ray scoring for rats at 15-wk post-surgery. 0 = no bony callus, 1 = partial healing across the gap, 2 = complete callus bridging across the gap, based on T-MG, by Chu et al.²² (C) μCT of rat midshaft femoral defects at 15-wk post-surgery. (D) Widest callus diameter measured in histological sections shown in panel E. (E) MacNeal's staining of the fractured femur indicates presence of more bone in calluses of TPO-treated rats compared to BMP-2 or saline treated rodents. Arrows indicate mineralization at the boundary between the scaffold and pin in TPO group. (F and G) Quantitation of callus area and % bony callus, respectively. While callus area is not significantly different, the percentage of bone tissue in the calluses is, with TPO having greatest percentage of bony callus. (H) Rat CSD study flow chart conducted on Long Evan males. Data in panel B compared by Kruskal–Wallis test due to nonparametric data distribution. Data in panels D, F, and G are parametric and therefore were compared by one-way ANOVA with Tukey–Kramer post-hoc test, * = $p < .05$, ** = $< .01$. "S" indicates scaffold in panel E.

study and were randomly assigned into treatment groups. All investigators were blinded to the treatment group while outcome analyses were completed.

Rodent X-rays (CSD)

Rodents were anesthetized using isoflurane inhalation and quickly transferred to the X-ray chamber in the prone position, being careful to isolate the surgical leg in the beam path. X-rays taken with a Faxitron machine (PiXarray 100, BioOptics Inc.) and images cropped to include proximal and distal ends of the femur. Scoring of X-ray images was conducted based on T.M.G. Chu et al., whereby a score of 0 = no healing or callus formation, 1 = partial healing or partial callus, and 2 = healed fracture with callus bridging.²²

μCT

Rodent CSD

Bones were dissected and fixed as above, then stored in 70% alcohol at 4°C until imaging. Bones were scanned using a SkyScan 1172 μCT (SkyScan) with the following parameters: 60 kV, 167 μA , 9.83 μm voxel size, Al filter of 0.5 mm,

rotation step of 0.7°, and frame averaging of 2. A hydroxyapatite phantom was used for calibration purposes. Individual slices were reconstructed using NRecon software (v.1.7.3), and 3D visualization was performed using CTVox software from SkyScan. Images were exported as TIFF files and scaffolds manually colored. A threshold of 110 (711 mg/cm^3 of hydroxyapatite as determined by the calibration phantoms) was used to determine the presence of mineralized tissue that formed 15 wk following surgery at the fracture site, which was higher than that used in the closed mouse fracture model intended to measure callus healing at 3 wk post-surgery.

Closed mouse fracture

Fracture healing was assessed using a Quantum FX μCT (Perkin Elmer). The μCT was scanned at high resolution with a voxel size of 10 μm . A phantom was used for calibration purposes. The Perkin Elmer quantum FX μCT (Perkin Elmer) was run at 90 kV and 88 μA , with a 14-min scan time and an Al 0.5 mm + Cu 0.06 mm filter. The scanning detector rate was 117 fps. The images were analyzed in ImageJ using the BoneJ package. In ImageJ, a grayscale threshold of 45

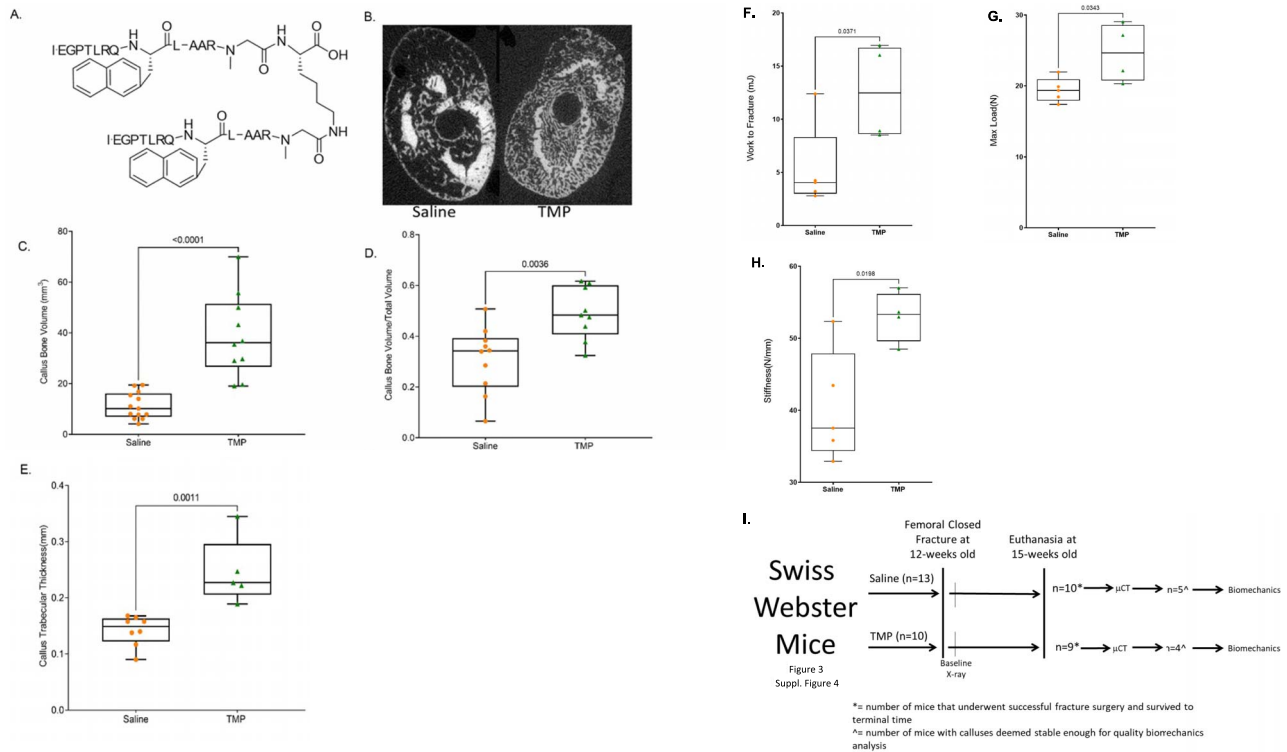
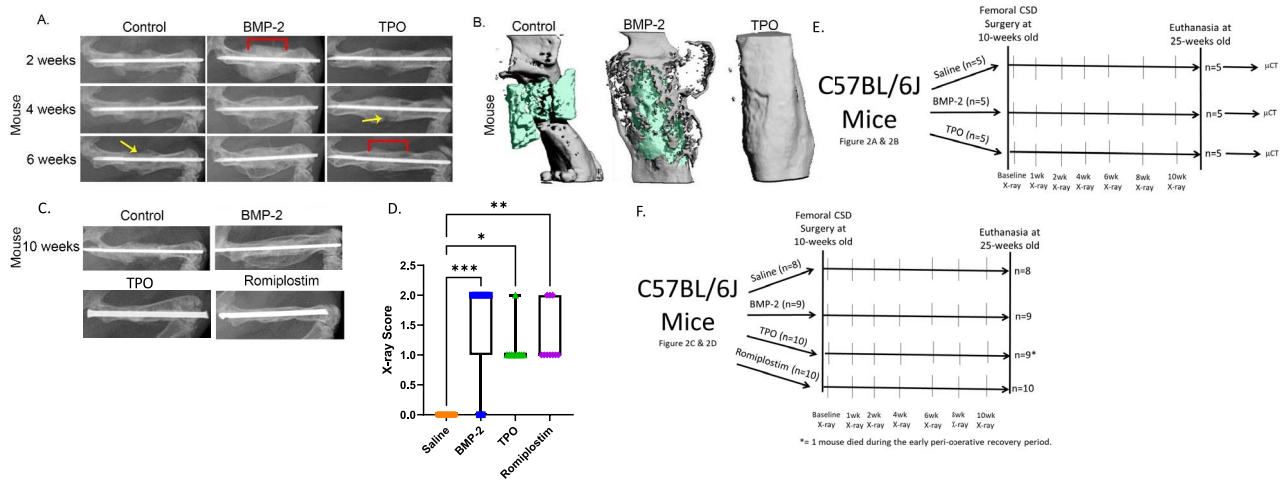


Figure 2. Thrombopoietic agents promote bone healing in mouse CSD models. Ten-wk-old, male C57BL/6J mice underwent CSD surgeries ($n = 5/\text{group}$). (A) Representative X-rays of mouse femurs 2-, 4-, and 6-wk post-surgery with control (saline), BMP-2 ($4 \mu\text{g}$), or TPO ($1 \mu\text{g}$) scaffolds. DCPD cement was used to carry the drugs. Periosteal bridging evident in 4- vs 6-wk TPO femurs. Arrows: unhealed periosteum; brackets: bridged callus. (B) Representative μCT reconstructions of mouse midshaft femoral defects 15-wk post-surgery, with control (saline), BMP-2 ($4 \mu\text{g}$), or TPO ($1 \mu\text{g}$) scaffolds (green). DCPD cement was used to carry the drugs. (C) Representative X-rays of mouse femurs 10-wk post-surgery with control (saline), BMP-2 ($1 \mu\text{g}$), TPO ($5 \mu\text{g}$), or romiplostim ($25 \mu\text{g}$). A collagen sponge secured around the scaffold was used to carry the drugs. (D) Bridging X-ray scoring for mice at 10-wk post-surgery. 0 = no bony callus, 1 = partial healing across the gap, 2 = complete callus bridging across the gap, based on TMG, by Chu et al.²² Each therapy induced more partial or full healing of fracture compared to control mice, as would be expected in a CSD model. (E) Experimental design flow chart for murine CSD experiments shown here in Figure 2A and B. (F) Experimental design flow chart for murine CSD figures shown here in Figure 2C and D. Nonparametric data compared by Kruskal–Wallis test. * = $<.05$, ** = $<.01$, *** = $<.001$. $n = 8$ saline, $n = 9$ BMP-2 and TPO, $n = 10$ for Romiplostim.

Figure 3. TMP promotes bone healing in a closed fracture model. Female Swiss Webster mice were 12 wk of age when subjected to Einhorn fracture. (A) Structure of TMP. (B) Transverse μCT slice through fracture callus 3-wk post-surgery. (C–E) μCT analyses showed that treatment with 33 nmol/kg/d of TMP significantly increases multiple fracture callus properties compared to vehicle controls (saline). (F–H) Biomechanical testing demonstrated that treatment with 33 nmol/kg/d of TMP ($n = 4$) significantly increased the amount of energy the healed femur absorbed before it re-fractured (F), the maximum load to failure (G), and the stiffness (H) compared to saline controls ($n = 5$). (I) Experimental design flow chart for female Swiss Webster mouse data shown here in Figure 3 and Figure S4. All statistical comparisons performed via Student’s t -test.

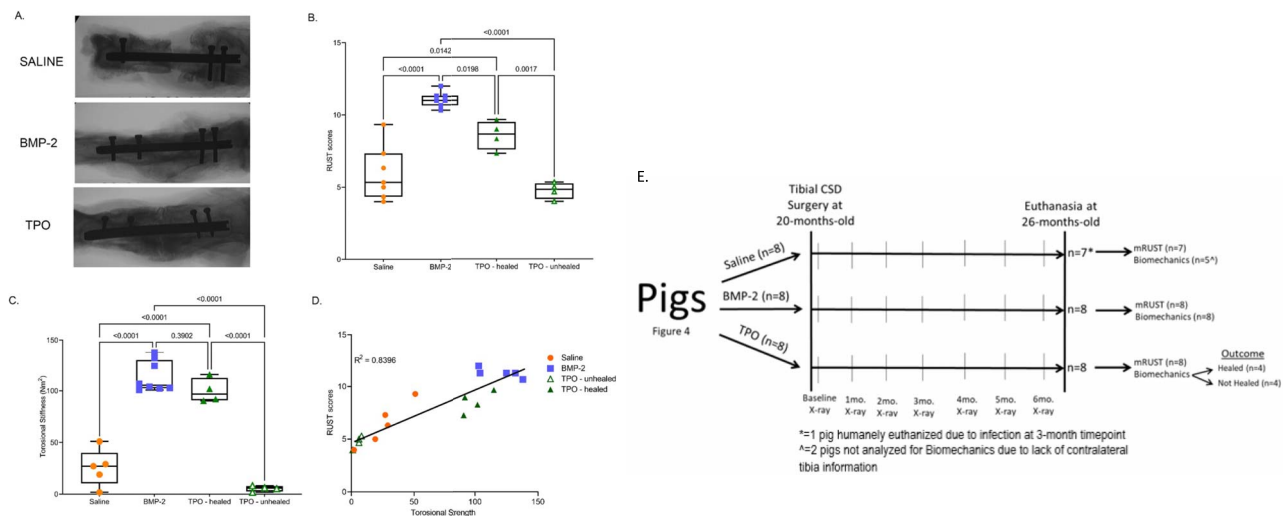


Figure 4. TPO promotes bone healing in a pig CSD model. Skeletally mature Yucatán miniature pigs were approximately 20 mo of age at the time of CSD surgery. (A) X-ray of pig tibial CSD, 6 mo post-surgery with control ($n = 7$), 1.5 mg BMP-2 ($n = 8$), or 1.5 mg TPO treated scaffolds ($n = 8$ total; $n = 4$ healed and $n = 4$ not healed). A collagen sponge secured around the scaffold was used to carry the drugs. (B) Radiographic union score for tibial fractures (RUST score) indicates that all BMP-2 treated pigs healed, 4 of 8 TPO treated pigs healed, and none of the saline treated pigs healed. (C) Torsion stiffness of operated tibia as a percentage of contralateral tibia confirms healing/non-healing RUST scores. Significant differences determined by ANOVA with Tukey–Kramer post-hoc test. (D) Correlation between RUST score and torsional stiffness determined by Pearson’s correlation test demonstrates an R^2 value of 0.8396. (E) Experimental design flow chart for male Yucatán miniature pig CSD data shown here in Figure 4.

(380 mg/cm³ of hydroxyapatite as determined by the calibration phantoms) was used to determine the presence of mineralized callus. Morphometric parameters were quantified in a prespecified region of interest (ROI) that included just the fracture callus. Trabecular thickness (Tb.Th), trabecular separation (Tb.Sp), total volume (TV), and volume of calcified callus (BV) were calculated.

Rat histology (CSD surgeries)

Fifteen weeks following surgery, rat surgical femurs were dissected and debrided of soft tissue attachments, being careful to avoid disturbing healing calluses and scaffolds. Bones were fixed in 10% neutral buffered formalin for 72 hr. Thereafter, tissue was dehydrated in graded concentrations of ethanol (70%, 80%, 85%, 90%, 95%, 100%—approximately 24 hr in each), followed by 50% ethanol and 50% methyl methacrylate (MMA) for 24 hr. Bones were then embedded in 100% MMA and thin slices (8 μ M) sectioned and then underwent MacNeal’s staining in batches (saline and BMP-2 samples in batch 1, followed by TPO samples in batch 2). Of note, histological sectioning procedures for callus evaluation were designed by the then Director of our Bone Histology Core, Dr. David Burr. Briefly, specimens were trimmed, and sections discarded until the edge of the callus was visible. Every fifth section was then collected until the center of the bone marrow cavity was reached (widest bone marrow diameter). The widest callus diameter, callus area, and % bony callus were then measured from these sections and analyzed using Image J software.

Mouse (closed fracture surgeries) biomechanical testing

Fractured femurs were tested for strength in a four-point bend to failure using an Instron dual column 5960 (Instron, Norwood, MA) with a 500 N load cell. Lower supports were 10 mm apart on the anterior face of the femur in contact with the proximal and distal diaphysis. Upper supports were

4 mm apart and spanned the entire fracture callus on the diaphysis. Force was applied from the posterior face of the femur with a displacement rate of 0.3 mm/s. We report the stiffness, maximum load, and work to fracture data that were generated. Of note, femurs that were grossly non-intact (as determined by manual manipulation) were excluded from biomechanical testing.

Pig RUST scoring

Six months following CSD surgery, pigs were euthanized and surgical tibiae dissected wrapped in saline-soaked gauze. Images were obtained using a fluoroscope (Philips BV Pulsera C-arm, Philips) to include orthogonal views of the tibial diaphysis (anterior, posterior, medial, and lateral). Fracture healing was assessed using the Radiographic Union Score for Tibial Fractures (RUST) method. Each cortex was given a score from 1 to 3 (1 = not healed, 2 = partial union, 3 = complete cortical union), and the scores summed for each animal ranging from 4 (no healing) to 12 (complete healing).²⁷

Platelet measurements

Rodents

Peripheral blood ($\sim 50 \mu$ L) was obtained from mice via tail vein in an EDTA tube (Becton Dickinson) at the time of CSD surgery (prior to incision), 2 wk after surgery, and 15 wk after surgery. Complete blood count (CBC) analysis was completed on the HEMAVET 950FS Hematology System (Drew Scientific). Of note, the first TPO bone healing studies completed by our team were the rat pilot studies. It was not until after those studies were conducted that we began collecting peripheral blood for platelet analysis, which was subsequently completed in mice and pigs.

Yucatán minipigs

Peripheral blood (~ 3 mL) was obtained from the jugular vein from each pig prior to initial skin incision on the day of the CSD surgery, 2 wk following surgery, and 3 mo following

surgery in a purple top EDTA tube (Becton Dickinson). CBCs from each sample were completed (ANTECH Diagnostics).

Microarray

Whole bone marrow and collagenase-digested femurs (90 min of incubation, see procedure below) of 12-wk-old male C57BL/6J mice were cultured with saline, BMP-2 (200 ng/mL), or TPO (100 ng/mL) for 48 hr. Total RNA was extracted using RNeasy Mini kit (QIAGEN), and quantified and qualified using the BioAnalyzer (Agilent Technologies, Inc.). The RNA integrity number (RIN) of all the samples was more than 8. Next, these mRNA samples were processed by the whole mouse genome cDNA microarray with $n = 4$ /group following the protocol described earlier.²⁸ The microarray slides from Agilent contained 44 000 probes, including more than 26 000 unique mouse genes covering the whole mouse genome. Purified RNA of interest and reference RNA (Agilent Technologies, Inc.) was labeled with Cy-5 and Cy-3, respectively. The labeled samples were simultaneously hybridized on a cDNA array for 17 h at 55 °C. After hybridization, slides were processed in a series of washes and scanned using an Agilent DNA microarray scanner. Features were extracted using the default setting of the Feature Extraction software v.11.5.1.1 (Agilent Technologies, Inc.).

GeneSpring v.14.9 (Agilent Technologies, Inc., RRID:SCR_010972) was used for data quality control, intra-chip normalization was completed using the locally weighted scatter-plot smoothing method (LOWESS), and statistical analysis.

Principal component analyses of microarray readouts were generated and visualized using GeneSpring v.14.9 (Agilent Technologies, Inc., RRID:SCR_010972). DEGs were curated by two selection criteria: (1) fold change >1.5 , where the fold change was defined by the ratio of gene expressions between TPO and saline, BMP-2 and saline, or BMP-2 and TPO; and (2) the moderate t -test $p \leq .05$. Pathway analysis using the DEGs was complete using Ingenuity Pathway Analysis software (Qiagen, RRID:SCR_008653), and the pathways meeting the hypergeometric t -test $p < .05$ were curated. The regulations of the pathways were determined by their z -scores. We defined that the networks with z -score greater than and lower than 1.0 were activated and inhibited, respectively. A panel of genes relevant to this study was validated by RT-PCR as detailed below.

Microarray validation using real-time PCR

RNeasy Mini kit (QIAGEN) was used to isolate RNA, and cDNA was synthesized using the QuantiTect Reverse Transcription Kit (Qiagen) using total RNA as per recommendations. Quantitative real-time PCR using QuantitectSYBR Green PCR Master Mix (Qiagen) was performed on a Quantstudio Real-Time PCR Detection System (CA). Table S1 contains the primers with sequences for the genes examined: angiopoietin 1 (ANGPT1), cyclin dependent kinase inhibitor 1A (CDKN1A), platelet and endothelial cell adhesion molecule 1 (PECAM1), protein phosphatase 1 regulatory inhibitor subunit 16B (PPS16B), vascular endothelial growth factor receptor 1 (FLT-1), SRC proto-oncogene, non-receptor tyrosine kinase (SRC), C-X-C motif chemokine ligand 10 (CXCL10), extracellular signal-related kinase 3 (ERK3), platelet factor 4 (PF4), and PDGF subunit B (PDGFB). The glyceraldehyde-3-phosphate dehydrogenase (GAPDH) gene served as the internal control. Melting curve analysis was used to confirm that each primer pair produced a

single amplification product. Relative gene expression was calculated using the $2^{-\Delta\Delta CT}$ method.²⁹

Antibody arrays

Following euthanasia, the midshaft of CSD mouse femora were isolated (-2 mm on each end of the femur), cleared of soft tissue, and stored at -80 °C. For protein isolation, femora were suspended in $1 \times$ RIPA buffer containing Halt Protease & Phosphatase Inhibitors (ThermoFisher Scientific, #78425) and homogenized using a Bullet Blender (Next Advance) in Navy RINO tubes at 4 °C for two consecutive, 5-min cycles. Following centrifugation (15 min at 14 000 rpm at 4 °C), supernatants were analyzed using a BCA Assay Kit (ThermoFisher Scientific, #23235) for determining protein concentration, and 50 μ g total protein lysate for each sample (saline $n = 4$, TPO $n = 4$, BMP-2 $n = 3$) was examined by multianalyte phospho-profiling arrays as previously described.³⁰ Briefly, lysates were applied to the TGF-beta Phospho Antibody Array (Full Moon Biosystems, #PTG176) according to the manufacturer's directions using Cy3-streptavidin (ThermoFisher Scientific, #434315) with the following modification: incubations were carried out at 4 °C in the protein labeling and coupling steps. Signal intensity was determined by Full Moon Biosystems on a GenePix 4000B scanner imager using GenePix Pro software and normalized against GAPDH, or the total amount of each specific protein as indicated in the text.

Additional materials and methodological information can be found in the Supplementary Information for the following experiments: isolation of CD45-CD31+ cells, angiogenesis assays, and vessel-like formation assay. Angiogenesis was analyzed using primary mouse bone marrow endothelial cells (BMECs) from 6-wk-old males as previously described.^{22,31,32}

Statistical analysis and study design

The animal study design for each experiment is described in the legend of appropriate figures.

Statistical analyses as well as assessments of data normality were performed with GraphPad Prism (version 8 and 10, GraphPad Software, RRID:SCR_002798). Results are displayed as mean \pm SD or Box and Whisker plots with lines at the median. To compare two groups of parametric data, a two-tailed Student's t -test was used. To compare three or more groups, a one-way ANOVA with Tukey-Kramer post hoc test was performed for parametric data; if the data were determined to be nonparametric, then they were compared via Kruskal-Wallis test with a Dunn's multiple comparison post-hoc test. p -values $< .05$ were considered significant. A Pearson's correlation test was used to determine linear relationships between sets of data.

Minimum numbers of mice and pigs were used in fracture healing studies and were determined using power calculations as detailed below. Please note that initial studies in rats were viewed as pilot studies and not included in these calculations. For mouse and pig CSD studies, our primary outcome was radiographically scored bone healing, and a power analysis was performed based on earlier work with a rat CSD model.³³ In their study, radiographic bone healing scores in control groups showed virtually no healing as would be expected in a CSD model (1 of 32 rats, or 3.125%). With use of rhBMP-2, maximal radiographic bone healing scores were observed in all 16 rats (5 of 5 for their scale). Therefore, for two-tailed

comparisons, 6 animals would be needed per group for an alpha significance of 0.05 and a power of 0.80. To account for animals that do not survive surgery or were excluded due to complications, 8-10 mice and 8 pigs were used per group. For Einhorn mouse fracture studies, Max Load was used as our primary biomechanical outcome, and BV/TV from μ CT analysis was used as our secondary outcome. We selected our biomechanical variable as our primary outcome, as it is the gold standard for bone healing. Based on the variance seen in our previous mouse μ CT and 4-point bend biomechanical experiments,²⁶ we found that for two-tailed comparisons, 7 animals would be needed per group for an alpha significance of 0.05, and a power of 0.80. Again, to account for mice that do not survive surgery or were excluded due to complications, 10-13 animals were used per group.

Results

TPO treatment enhances bone healing in rodent femoral CSD models

Based on the anabolic regulation of bone formation by MKs,¹⁰ we sought to determine whether local administration of TPO at the time of surgery enhances bone healing. This timing/route of administration mimics current clinical usage of BMP-2. In a pilot study using male Long Evans rats, clear bridging callus formation was observed by X-ray and μ CT imaging with both BMP-2 and TPO treatment in bones retrieved 15 wk post-surgery (Figure 1A and C). X-ray scoring of the bones using methods by T-MG. Chu et al.²² demonstrated significantly greater healing in BMP-2 and TPO-treated animals compared to saline-treated controls (Figure 1B). Additionally, BMP-2 treatment resulted in a large callus that is not completely mineralized (Figures 1D-G). On the other hand, the bridging callus in the TPO group had a thicker cortex, smaller diameter, and more physiologic contour than the BMP-2 group, suggesting different healing modalities between these agents (Figure 1A and C-G). Representative images and quantitation of rat bone calluses stained with MacNeal's showed that callus areas are not different among the groups (Figure 1E and F), but the callus diameter at the widest point trended narrower in the TPO-treated group as compared to that observed in the saline and BMP-2 treated groups (Figure 1D and E, $p = .13$). Yet the percentage of bone within the callus was significantly higher in the TPO-treated animals; the BMP-2 treatment also increased the percentage of bony callus compared to saline treatments, but not to the extent that the TPO therapy did (Figure 1E and G). In a mouse femoral CSD model, the average time to obtain bridging callus formation in BMP-2 treated mice (4 μ g, positive control) was 2 wk, which was several weeks earlier than TPO-treated mice (1 μ g) (Figure 2A). However, both BMP-2 and TPO treatment resulted in bridged callus by 6 wk; saline-treated (negative control) scaffolds failed to form a bridged callus, even 15 wk post-surgery (Figure 2A-C). Importantly, these data establish that TPO can stimulate CSD healing in rodents.

TPO-mimetics enhance bone healing

To further examine the translational nature of using thrombopoietic agents for bone healing, we examined the use of a collagen sponge carrier (vs cement used in the studies above, Figures 1 and 2A and B) and the FDA-approved second-generation TPO-mimetic romiplostim. These studies

revealed that romiplostim (25 μ g) was capable of stimulating healing of a mouse CSD after 10 wk (Figure 2C and D). As expected, BMP-2 and TPO also stimulated bone healing, whereas saline did not. X-ray scoring analysis confirmed the qualitative healing observed with the three different therapies (Figure 2C and D). Of note, one mouse died during the early peri-operative recovery period within the TPO-treated group, as indicated in Figure 2F.

While promising, without dosing studies, it is premature to speculate about effective doses in humans. However, based on our results, to augment bone healing would likely exceed the 1500 μ g of romiplostim provided to patients each week, but a single dose implanted at the time of surgery would be far less than a total cumulative life-time dose of 78 000 μ g currently used systemically without serious drug-related sequelae.³⁴

Systemic delivery of TMPs enhance bone healing

Next, we investigated if TMPs could stimulate bone healing in a closed fracture model with systemic administration. TMP—AF13948 is a stabilized dimer of AF12505 (Figure 3A), a synthetic peptide Mpl agonist that has almost equal TPO activity as the whole TPO protein.¹⁵ It was discovered by directed evolution of phage³⁵ and has been demonstrated to have particularly high potency and stability and was synthesized to be used as a systemically administered drug. TMPs are 14 amino acid branched chain synthetic peptides (Figure 3A), which illicit the biological response of TPO.^{15,36} Dosing studies showed that TMPs improved bone healing (Figure S4). During the course of this study, a total of 4 mice died (3 in the saline group and 1 in the TMP group) during the post-operative period prior to the 15-wk terminal time point. Quantitative μ CT analyses with the optimal dose (33 nmol/kg/d, S.Q. for 3 wk) demonstrated that TMP treatment ($n = 9$) resulted in a significant increase in mineralized tissue in the callus compared to vehicle treatment ($n = 10$) ($245 \pm 42\%$), due in part to significant increases in bone density ($59 \pm 17\%$) and Tb.Th ($74 \pm 17\%$) in the callus (Figure 3B-E). Next, biomechanical testing was completed in appropriately intact specimens as described above. This yielded 4 TMP-treated and 5 saline-treated samples, which were able to undergo biomechanical testing (40.0% and 38.5% of specimens, respectively). In TMP-treated mice, the increase in mineral deposition led to a marked improvement in the overall strength of intact fractured femurs with a greater than 2-fold increase in work to fracture (Figure 3F), a $27 \pm 10\%$ increase in maximum load (Figure 3G) endured before failure, and a $31 \pm 6.6\%$ increase in stiffness (Figure 3H).

TPO can heal a CSD in a large animal model

Motivated by promising rodent data, we sought to further test thrombopoietic agents in a large animal model. We chose adult Yucatán miniature pigs due to their similar body weight to adult humans, the availability of implants that are used clinically, and the similarity of pig bone and blood physiology to humans.³⁷ A CSD was created in the right tibia and treated with saline, 1.5 mg BMP-2, or 1.5 mg TPO delivered by an FDA-approved sponge for BMP-2 delivery (Medtronic/Integra Life Sciences). Figure S3 shows the pig surgery and tibia with the scaffold held in place using an intramedullary nail ($n = 8$ pigs/group). Following surgery, 1 pig developed an infection at the surgical site, which could not be managed; this animal was euthanized prior to the study endpoint of 6 mo per advice from the attending veterinarian. Healing

was assessed following examination of X-rays (Figure 4A) using the RUST score (4 minimum to 12 maximum) and through biomechanical testing (Figure 4B-D). Saline-treated pigs did not heal (RUST score: 6.0 ± 1.7), whereas all 8 pigs treated with BMP-2 did heal (RUST score: 11.1 ± 0.5). In the TPO group, 4 animals healed (RUST score: 8.6 ± 0.9) and 4 animals did not heal (RUST score: 4.8 ± 0.5). Non-destructive torsional testing was completed to measure the percent torsional stiffness in the operated tibiae compared to the non-operated contralateral tibiae. All operated tibiae in the BMP-2 treated group healed, as demonstrated by a torsional stiffness of $114 \pm 15\%$. Conversely, all of the operated tibiae in the saline-treated group remained unhealed with a torsional stiffness of $26 \pm 13\%$. Interestingly, 4 of 8 tibiae in the TPO-treated group healed with a torsional stiffness of $100 \pm 12\%$. However, 4 of 8 tibiae in the TPO-treated group did not heal ($5 \pm 6\%$). The torsional stiffness in the unhealed TPO group was not significantly different from the saline group ($p = .06$). RUST scores and torsional stiffness scores showed a strong correlation (Figure 4D), which was used to subdivide the TPO group (healed vs unhealed). While this single, unoptimized TPO dose did not heal all pigs, it is possible that optimizing dosing and/or timing would allow more pigs to heal. To this point, we observed no CSD healing in 3 of 3 animals treated with a higher TPO dose (7.5 mg, data not shown), suggesting that the bone healing benefits of locally delivered TPO are abolished at high concentrations.

To summarize our data thus far, we have shown that thrombopoietic agents are capable of augmenting bone healing across 3 animal models (mouse, rat, and pig), using multiple classes of agents (recombinant TPO, small molecule agonist, and synthetic peptide mimetics), and through local and systemic delivery mechanisms.

Platelet concentrations following local delivery of TPO

Because thrombopoietic agents are used clinically to increase platelets, we examined whether a single local dose of TPO at the time of surgery impacts circulating platelet concentrations in mice and pigs. For mice, platelet concentrations were not significantly different between pre-surgical values at 2 wk and 15 wk post-surgery (1103 ± 132 , 1086 ± 146 , and 1034 ± 75 , respectively) (normal range: $732\text{--}1160 \times 10^3/\mu\text{L}$).³⁸ For pigs, a similar trend was observed: pre-surgery (445 ± 63), 2 wk post-surgery (540 ± 44), and 3 mo post-surgery (487 ± 92) (normal range: $311\text{--}585 \times 10^3/\mu\text{L}$).³⁹ These data suggest that a single, local delivery of TPO is sufficient to stimulate bone healing, but did not lead to a sustained elevation of circulating platelets.

TPO stimulates a greater number of growth factor cytokine pathways than does BMP-2

Bone healing requires stimulation of multiple anabolic pathways in bone marrow mesenchymal and hematopoietic cells. In order to understand some of the similarities and differences between BMP-2 and TPO in this regard, we treated collagenase-digested bone cells and bone marrow from mouse femurs with BMP-2 (200 ng/mL), TPO (100 ng/mL), or saline for 48 hr and collected total RNA for microarray analysis. From these heterogeneous preparations, we found remarkably different profiles of gene expression changes between the two treatments (Figure 5A and B). Ingenuity Pathway

Analysis of differentially expressed genes (DEGs) in the BMP-2 and TPO groups vs saline revealed angiogenesis as a major pathway affected by these two agents, with the majority of genes regulated by TPO. Additionally, TPO treatment resulted in the upregulation of numerous growth factors and cytokines compared to BMP-2 (eg, VEGF, angiopoietin, and PDGF, Tables S2, S3, and S6), many of which are known to participate in bone healing.⁴⁰ Consistent with this, multianalyte phospho-profiling arrays using protein from mouse femora subjected to fracture and treated for 3 d with saline, BMP-2, or TPO (5 μg each via collagen sponge) revealed broader regulation of effector phosphorylation status with TPO as compared to BMP-2 (Tables S4 and S5). For instance, increased activation-related phosphorylation of AKT1 and AKT2, which are downstream of several of these growth factors and cytokines, was observed with TPO treatment but not BMP-2 treatment (Figure 5C and D). Similarly, we measured increased activation-related phosphorylation of MAP kinase pathway components (MKK3, MEKK1) with TPO-treatment (Tables S4 and S5) but not BMP-2. Finally, phosphorylation of PAK1, which is involved in actin cytoskeletal dynamics and motility, was increased with TPO treatment but not BMP-2 treatment (Figure 5E). These molecular signals are consistent with broader activation of healing pathways by TPO treatment compared to BMP-2 treatment.

TPO stimulates endothelial cell proliferation *in vivo* and *in vitro*

Three weeks post-surgery, mice treated with TPO or BMP-2 had a significantly higher percentage of CD45-CD31+ endothelial cells within the bone regenerate than did saline-treated mice (Figure S5). Of note, given the restricted pattern of Mpl expression, we first used qPCR to confirm its expression in CD45-CD31+ endothelial cells (cell digested from the bone regenerate or bone/callus in the fracture defect region). Mpl was found to be robustly transcribed in these cells as compared to the CD45-CD31- population (Figure S6), consistent with prior reports showing that endothelial cells express Mpl.⁴¹

Next, we investigated the effect of TPO on bone marrow endothelial cells (BMECs) *in vitro*. Specifically, to test the effect of TPO on BMECs, we looked at several cellular parameters using validated 2D culture assays.^{22,31,32,42,43} TPO significantly increased cell number and the length of vessel-like structures/tube length in WT BMECs (Figure 6A and B). However, TPO treatment did not increase cell number or vessel-like structure length (tube length) in Mpl KO BMECs (Figure 6A and B), showing the importance of Mpl expression in TPO-induced increases. Consistent with prior studies,⁴⁴ BMP-2 treatment stimulated a trending increase in WT BMEC number and a significant increase in vessel-like structure length (Figure 6A and B). It is unclear why BMP-2 did not increase BMEC number or vessel-like structure length in the absence of Mpl expression. It is possible that BMP-2 stimulates autocrine signaling through the Mpl receptor, but this requires further study (Figure 6A and B).

Discussion

Fracture non-unions represent an ongoing clinical challenge. Compared with properly healed fractures, non-unions account for an outsized proportion of morbidity for patients

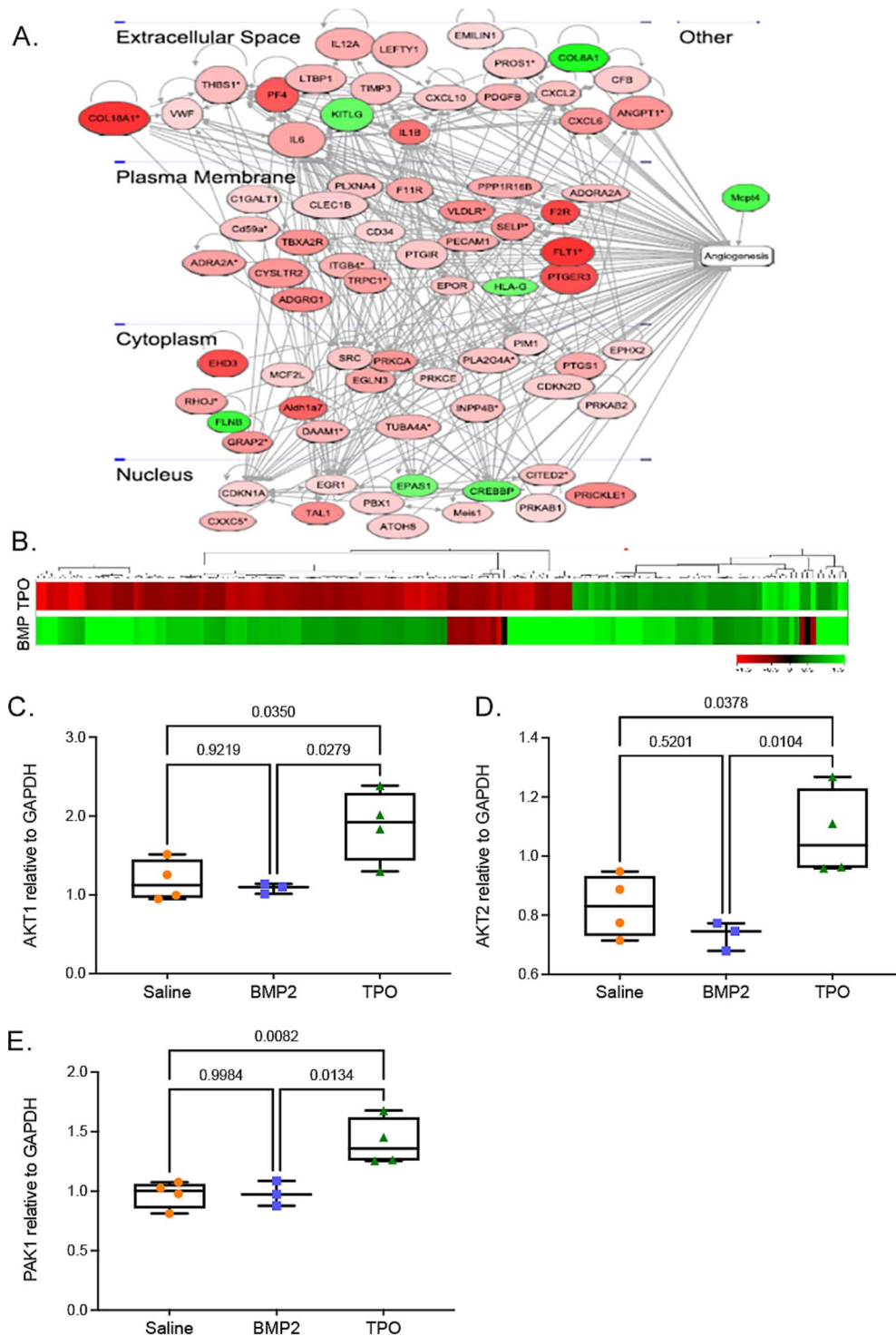


Figure 5. TPO promotes the upregulation of the angiogenesis pathway and growth factor activation. Bone/bone marrow cells were cultured with saline, BMP-2 (200 ng/mL), or TPO (100 ng/mL) for 48 hr and were processed for transcriptomic analysis ($n = 4$ /group). (A) Functional network analysis found the angiogenesis pathway, as one of the key differential markers between BMP-2 and TPO treatment. The angiogenesis pathway was significantly activated in TPO treated samples (z -score = 1.15) but inhibited in BMP-2 treated samples (z -score = -1.86). Genes enriching the angiogenesis pathway are listed in Table S2. Network shown for TPO treatment only. Oval shaped nodes represent DEGs. (B) The color key with respect to genes log₂ (fold change) is shown at the bottom of the network for TPO and BMP-2; red and green colored genes were upregulated and down regulated, respectively. Genes are clustered into cellular compartments where the corresponding proteins are typically expressed. (C-E) Fracture callus was assessed 3-d post-surgery for mice treated with saline, BMP-2 (5 μ g), or TPO (5 μ g) and was then examined by multi-analyte TGF-beta phospho-profiling arrays ($n = 4$ /group). TPO increased activation of AKT1 (C), AKT2 (D), and PAK1 (E), whereas BMP-2 did not. Significant differences were determined by ANOVA with Tukey-Kramer post-hoc test.

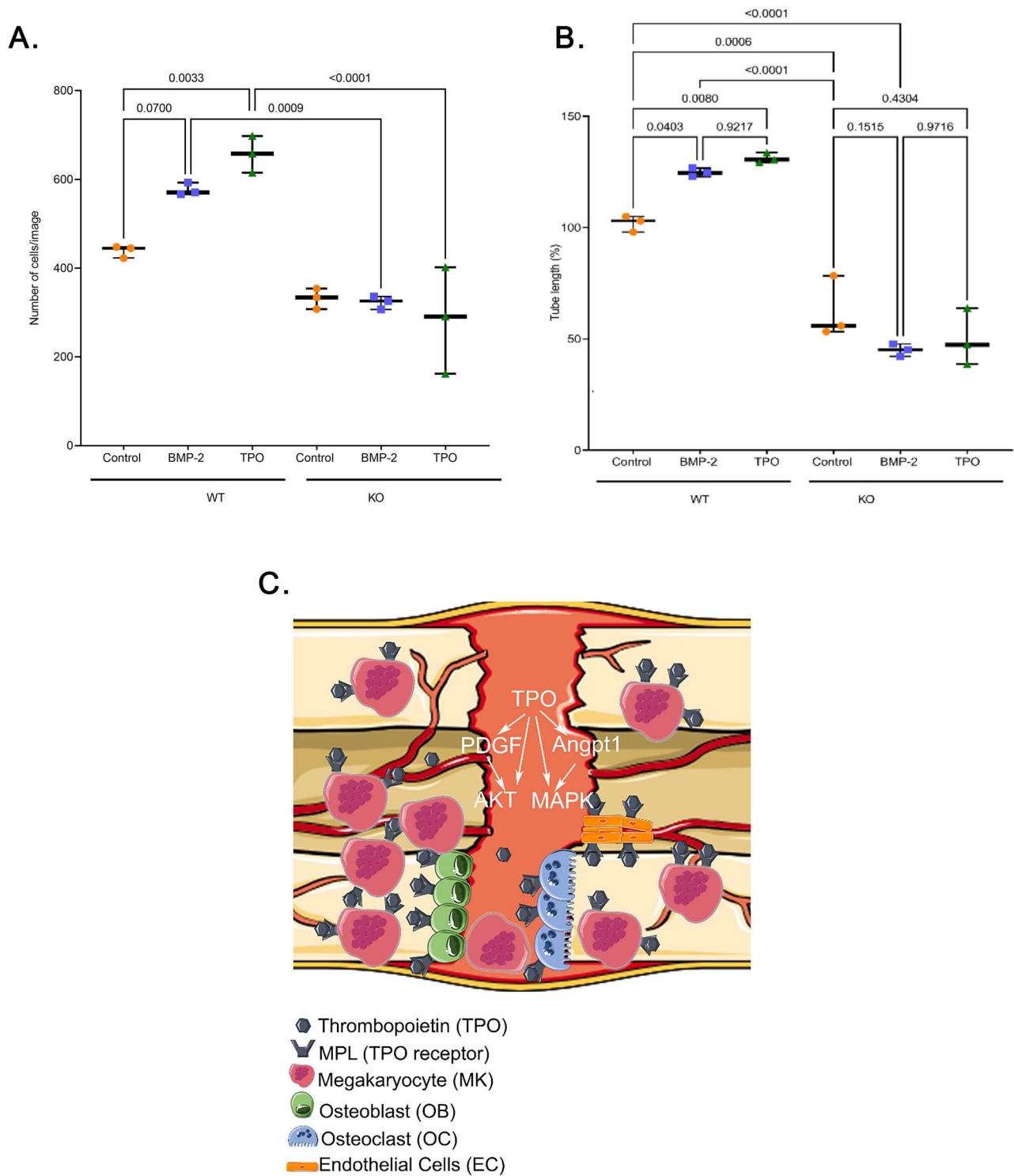


Figure 6. TPO treatment promotes endothelial cell growth in vivo and in vitro. (A and B) Treatment of WT bone marrow endothelial cells (BMECs) with TPO (100 ng/mL) or BMP-2 (200 ng/mL) increased BMEC numbers (A) and vessel-like structure length or tube length (% relative to WT + saline control) (B). However, treatment of Mpl KO BMECs with TPO or BMP-2 did not increase BMEC numbers (A) nor tube length (B). Of note, cell number (A) and tube length (B) were significantly higher (or trending higher) in WT BMEC cultures compared to KO BMEC cultures with the same treatment ($n = 3/\text{group}$). Significant differences were determined by ANOVA with a Tukey–Kramer post-hoc test. (C) Working model as to how TPO stimulates angiogenesis and bone healing. TPO treatment upregulates the expression of PDGF, Angpt1, AKT, and MAPK, which can promote angiogenesis, a critical process of successful fracture healing. TPO also stimulates MKs, which increase osteoblast proliferation and bone formation. Further, TPO increases osteoclastogenesis, which is important to remove necrotic tissue and to remodel the fracture callus.

and financial burden on our health care system. Here, we show that thrombopoietic agents have potential as a novel bone-healing agent. The *in vivo* healing trajectory in conjunction with cellular and molecular studies strongly supports a unique mode of action from the currently FDA-approved treatment (BMP-2). In this work, we present evidence that multiple thrombopoietic agents (recombinant proteins, small-molecule agonists, and mimetic peptides) are capable of supporting fracture healing. Our cellular studies and the use of multiple agents strongly suggest that the Mpl receptor mediates this support by activation of a myriad of pathways. Clinically, TPO peptidomimetics and small-molecule Mpl agonists (used in this work) are approved for an unrelated blood disorder. Repurposing previously approved medications with an established safety profile to support fracture healing in at-risk patients is an attractive possibility.

We have shown that thrombopoietic agents stimulate bone healing in rodents and large animals. Indeed, local delivery of TPO stimulates bridging of CSDs in mice and rats. In both species, time to bridging was longer than that following treatment with BMP-2; however, the bridged fracture sites were more mineralized and lacked the large fracture callus associated with BMP-2. A similar dynamic was observed in the Yucatán pigs, for which bone healing occurred. Our bimodal pig data suggests the need to continue to optimize this potential treatment. Further supporting the need for optimization, a pilot study of 3 Yucatán pigs receiving 5× the TPO dose presented here failed to heal a similarly sized CSD (data not shown). This failure was likely due to excess resorption. Given the known side-effect profile of BMP-2, an optimized thrombopoietic agent treatment may achieve a better risk–benefit trade-off for CSD healing. Overall, the collection of agents used in this work, across multiple fracture models and multiple species, offers a novel treatment avenue for problematic fractures that appears conserved and robust.

Our transcriptomic analyses and cellular studies show that TPO enhances angiogenesis (Figures 5 and 6), which is required for successful bone healing. To the best of our knowledge, this is the first demonstration of exogenous TPO enhancing vessel formation in the context of fracture healing and is consistent with reports of TPO simulating vasculogenesis following ischemic injury⁴⁵ and vascular cell therapies enhancing fracture healing through increased perfusion to bone defects.^{46,47} Primary cells being harvested at 6 wk is indicative of cells from adolescent/young adult mice and is a common age for experiments using primary bone marrow stromal cells (BMSCs), osteoclast progenitors, and primary osteocytes.^{14,28–31,33,47} We recognize, though, that using cells isolated from older mice may lead to lower baseline angiogenesis in controls. However, published results demonstrate that BMEC angiogenesis can be induced in 70-wk-old mice (1.3 yr) by altering components of angiogenic pathways, even genes identified in our microarray, such as FLT-1 and PDGFb.⁴⁸ Also, we previously showed that TPO increased the number of vascular nodules and meshes in aged female BMECs, suggesting enhanced angiogenic connectivity and complexity, as well as increased expression of Angiopoietin 1 and 2 in mice of both sexes aged 22–24 mo.³³ Taken together, studies in older mice manipulating angiogenesis using TPO and other factors lead us to speculate that the benefit of treating fractures with thrombopoietic agents is preserved with age. While it is understood that

fracture healing is more efficient in younger animals, the cellular and molecular mechanisms of the healing process are conserved with age and similar across mammalian models of fracture.⁴⁹ However, this hypothesis of using thrombopoietic agents in aged mice to assist fracture healing remains to be formally tested. Similarly, the use of these agents in animals with comorbidities that delay healing (eg, diabetes, osteoporosis) remains to be examined.

Here, we also provide protein-level data (Figure 5C–E) showing TPO stimulates signal transduction events in pathways that are also upregulated in our gene expression studies. These data, and previously published results, suggest a model in which TPO stimulates bone healing via multiple pathways (Figure 6C). Specifically, TPO stimulates protein signaling that induces angiogenesis, a critical process of successful fracture healing. TPO also stimulates MKs, which in turn increase osteoblast proliferation and bone formation.^{10,12–14} Additionally, TPO increases osteoclastogenesis, which is important to remove necrotic tissue and to remodel the fracture callus.⁵⁰ Thus, thrombopoietic agents are capable of increasing angiogenesis, bone formation, and bone resorption—all processes fundamental to proper fracture healing.

As with most fracture studies, there are a number of limitations, including the exclusion of animals due to poor surgical outcome, death during the perioperative period, and sample processing issues. In addition, in our study, mechanical testing was only completed on femurs that were intact at the time of euthanasia. This reduced our sample size below what was required by power analysis, but even with this limitation, we still report significant changes. Conducting a full spectrum of biomechanical tests in these various groups of animals, including peak load, yield load, and displacement post-yield, would expand our understanding of the potential these thrombopoietic agents have to improve bone healing and quality. Finally, the complexity of large animal studies precluded thorough dose optimization studies.

Limitations notwithstanding, we showed the ability of TPO/TPO-mimetics to heal fractures and that mechanical testing showed improved healing compared to control CSD (Figures 1–4). Specifically, multiple laboratories within multiple institutions demonstrated the ability of TPO/TPO-mimetics to heal bones in three animal species (mice, rats, and pigs), two mouse strains (C57BL/6J and ND4 Swiss Webster), and in multiple injury models, including arguably one of the most difficult bone healing models, a CSD. We also administered thrombopoietic agents through multiple routes and, where applicable, with multiple drug carriers. Together, these data show the robustness of the results, supporting the usage of thrombopoietic agents in bone healing, which was further evidenced by cellular/molecular studies showing that thrombopoietic agents stimulate a multifaceted response to augment fracture healing. Finally, thrombopoietic agents are FDA-approved for platelet disorders, which suggests a rapid translational pathway for including bone healing as a new indication.

Acknowledgments

The presented contents are solely the responsibility of the authors and do not necessarily represent the official views of any of the aforementioned agencies. We would also like to acknowledge Dr. David Burr for his expertise regarding the histological/imaging assessments of the rodent studies and his input on the sample processing given some bones were damaged when pins were removed from mouse femurs. Finally,

we would like to thank Drs. David Waning and Amy Creecy for their assistance in addressing reviewer concerns and carefully reviewing the manuscript. Graphical abstract was created in BioRender (<https://BioRender.com>).

Disclaimer: The views, opinions, and/or findings contained in this report are those of the author(s) and should not be construed as official Department of the Army position, policy, or decision, unless so designated by other official documentation. Citations of commercial organizations or trade names in this report do not constitute an official Department of the Army endorsement or approval of the products or services of these organizations. This research complied with the Animal Welfare Act and implementing, Animal Welfare Regulations, the Public Health Service Policy on Humane Care and Use of Laboratory Animals and adhered to the principles noted in The Guide for the Care and Use of Laboratory Animals.

Author contributions

Paul J. Childress (Conceptualization, Data curation, Formal analysis, Funding acquisition, Investigation, Methodology, Project administration, Supervision, Writing—original draft, Writing—review & editing), Jeffery J. Nielsen (Conceptualization, Data curation, Formal analysis, Funding acquisition, Investigation, Methodology, Project administration, Supervision, Writing—original draft, Writing—review & editing), Thomas Bemenderfer (Data curation, Formal analysis, Investigation, Methodology, Writing—review & editing), Ushashi C. Dadwal (Conceptualization, Data curation, Formal analysis, Funding acquisition, Investigation, Methodology, Project administration, Supervision, Writing—original draft, Writing—review & editing), Nabarun Chakraborty (Conceptualization, Data curation, Formal analysis, Funding acquisition, Investigation, Methodology, Project administration, Supervision, Writing—original draft, Writing—review & editing), Jonathan S. Harris (Data curation, Formal analysis, Investigation, Methodology, Writing—review & editing), Monique Bethel (Data curation, Formal analysis, Investigation, Methodology, Writing—review & editing), Marta Alvarez (Data curation, Formal analysis, Investigation, Methodology, Writing—review & editing), Aamir Tucker (Data curation, Formal analysis, Investigation, Methodology, Writing—review & editing), Alexander R. Wessel (Data curation, Formal analysis, Investigation, Methodology, Writing—review & editing), Patrick D. Millikan (Data curation, Formal analysis, Investigation, Methodology, Writing—review & editing), Jonathan H. Wilhite (Data curation, Formal analysis, Investigation, Methodology, Writing—review & editing), Andrew Engle (Data curation, Formal analysis, Investigation, Methodology, Writing—review & editing), Alexander Brinker (Data curation, Formal analysis, Investigation, Methodology, Writing—review & editing), Jeffrey Rytlewski (Data curation, Formal analysis, Investigation, Methodology, Writing—review & editing), David C. Scofield (Data curation, Formal analysis, Investigation, Methodology, Writing—review & editing), Kaitlyn S. Griffin (Data curation, Formal analysis, Investigation, Methodology, Writing—review & editing), W. Christopher Shelley (Data curation, Formal analysis, Investigation, Methodology, Writing—review & editing), Kelli J. Manikowski (Data curation, Formal analysis, Investigation, Methodology, Writing—review & editing), Krista L. Jackson (Data curation, Formal analysis, Investigation, Methodology, Writing—review & editing), Stacy Ann Miller (Data curation, Formal analysis, Investigation, Methodology, Writing—review & editing), Ying-Hua Cheng (Data curation, Formal analysis, Investigation, Methodology, Writing—review & editing), Joydeep Ghosh (Data curation, Formal analysis, Investigation, Methodology, Writing—review & editing), Patrick L. Mulcrone (Conceptualization, Data curation, Formal analysis, Funding acquisition, Investigation, Methodology, Project administration, Supervision, Writing—original draft, Writing—review & editing), Edward F. Srouf (Conceptualization, Formal analysis, Funding acquisition, Project administration, Supervision, Writing—original draft, Writing—review & editing), Mervin C. Yoder (Conceptualization, Formal analysis, Funding acquisition, Project administration, Supervision, Writing—original draft, Writing—review & editing), Roman M. Natoli (Conceptualization, Data curation,

Formal analysis, Funding acquisition, Investigation, Methodology, Project administration, Supervision, Writing—original draft, Writing—review & editing), Karl D. Shively (Conceptualization, Data curation, Formal analysis, Funding acquisition, Investigation, Methodology, Project administration, Supervision, Writing—original draft, Writing—review & editing), Aarti Gautam (Conceptualization, Formal analysis, Funding acquisition, Project administration, Supervision, Writing—original draft, Writing—review & editing), Rasha Hammamieh (Conceptualization, Formal analysis, Funding acquisition, Project administration, Supervision, Writing—original draft, Writing—review & editing), Stewart A. Low (Conceptualization, Formal analysis, Funding acquisition, Project administration, Supervision, Writing—original draft, Writing—review & editing), Philip S. Low (Conceptualization, Formal analysis, Funding acquisition, Project administration, Supervision, Writing—original draft, Writing—review & editing), Todd O. McKinley (Conceptualization, Data curation, Formal analysis, Funding acquisition, Investigation, Methodology, Project administration, Supervision, Writing—original draft, Writing—review & editing), Jeffrey O. Anglen (Conceptualization, Data curation, Formal analysis, Funding acquisition, Investigation, Methodology, Project administration, Supervision, Writing—original draft, Writing—review & editing), Jonathan W. Lowery (Conceptualization, Formal analysis, Funding acquisition, Project administration, Supervision, Writing—original draft, Writing—review & editing), Tien-Min G. Chu (Conceptualization, Data curation, Formal analysis, Funding acquisition, Investigation, Methodology, Project administration, Supervision, Writing—original draft, Writing—review & editing), and Melissa A. Kacena (Conceptualization, Formal analysis, Funding acquisition, Project administration, Supervision, Writing—original draft, Writing—review & editing). This manuscript merges 4 large investigations from 7 laboratories at 4 different institutions. The junior researcher completing the majority of the studies within each of the 4 large investigations was designated co-first author. The order was determined based on the amount of time invested into each study. Paul J. Childress, Jeffery J. Nielsen, Thomas Bemenderfer, and Ushashi C. Dadwal are co-first authors.

Supplementary material

Supplementary material is available at *Journal of Bone and Mineral Research* online.

Funding

Funding for these studies was provided in part by: US National Institutes of Helath (AR060863 [M.A.K.], AR060332 [M.A.K.], DK007519 [P.J.C.], AG060621 [M.A.K.]), Indiana Clinical and Translational Sciences Institute (RR025761 [M.A.K., J.J.N.], TR000006 [M.A.K., T.-M.G.C.]), Orthopaedic Trauma Association [M.A.K., T.O.M.], US Department of Defense, USAMRMC (W81XWH-13-1-0407 [M.A.K.], W81XWH-13-1-0500 [J.O.A., T.O.M.], W81XWH-13-1-0501 [T.-M.G.C.]), Indiana University Health Values Grant [K.D.S.], Indiana University Collaborative Research Grant [M.A.K., J.O.A.], and Marian University Faculty Research Development Grant [J.W.L.]. This material is the result of work supported with resources and the use of facilities at the Richard L. Roudebush VA Medical Center, Indianapolis, IN: Veterans' Administration Merit Award #BX003751 [M.A.K.], Veterans' Administration Merit Award #BX006399 [M.A.K.], and Veterans' Administration Research Career Scientist Award #RX004809 [M.A.K.]. This work was also supported by Military Operational Medicine Research Program (Proposal # 24780 [R.H.]).

Conflicts of interest

M.A.K. and T.-M.G.C. are co-inventors on a patent for the use of thrombopoietic agents in bone healing. M.A.K. is the founder of OsteoFuse, LLC. For all other authors, no conflicts of interest exist.

Data availability

The gene database is available in GEO: GSE149329. The protein data are provided in the Supplementary Tables. All other datasets generated during and/or analyzed during the current study are available from the corresponding author upon reasonable request.

Ethics approval statement

Mouse, rat, and pig critical sized defect experiments were performed in accordance with protocols approved by Indiana University's Institutional Animal Care and Use Committee (IACUC). Closed fracture mouse studies were performed in accordance with protocols approved by Purdue University's IACUC.

References

- Loeffler J, Duda GN, Sass FA, Dienelt A. The metabolic microenvironment steers bone tissue regeneration. *Trends Endocrinol Metab.* 2018;29(2):99–110. <https://doi.org/10.1016/j.tem.2017.11.008>
- Einhorn TA, Gerstenfeld LC. Fracture healing: mechanisms and interventions. *Nat Rev Rheumatol.* 2015;11(1):45–54. <https://doi.org/10.1038/nrrheum.2014.164>
- Baht GS, Vi L, Alman BA. The role of the immune cells in fracture healing. *Curr Osteoporos Rep.* 2018;16(2):138–145. <https://doi.org/10.1007/s11914-018-0423-2>
- Pape HC, Marcucio R, Humphrey C, Colnot C, Knobe M, Harvey EJ. Trauma-induced inflammation and fracture healing. *J Orthop Trauma.* 2010;24(9):522–525. <https://doi.org/10.1097/BO.T.0b013e3181ed1361>
- Dickson K, Katzman S, Delgado E, Contreras D. Delayed unions and nonunions of open tibial fractures. Correlation with arteriography results. *Clin Orthop Relat Res.* 1994;302:189–193. <https://doi.org/10.1097/00003086-199405000-00029>
- Schlickewei CW, Kleinertz H, Thiesen DM, et al. Current and future concepts for the treatment of impaired fracture healing. *Int J Mol Sci.* 2019;20:22. <https://doi.org/10.3390/ijms20225805>
- Hustedt JW, Blizzard DJ. The controversy surrounding bone morphogenetic proteins in the spine: a review of current research. *Yale J Biol Med.* 2014;87(4):549–561.
- Yan XQ, Lacey D, Hill D, et al. A model of myelofibrosis and osteosclerosis in mice induced by overexpressing thrombopoietin (Mpl ligand): reversal of disease by bone marrow transplantation. *Blood.* 1996;88(2):402–409. <https://doi.org/10.1182/blood.V88.2.402.bloodjournal882402>
- Villeval JL, Cohen-Solal K, Tulliez M, et al. High thrombopoietin production by hematopoietic cells induces a fatal myeloproliferative syndrome in mice. *Blood.* 1997;90(11):4369–4383. <https://doi.org/10.1182/blood.V90.11.4369>
- Kacena MA, Shivdasani RA, Wilson K, et al. Megakaryocyte-osteoblast interaction revealed in mice deficient in transcription factors GATA-1 and NF-E2. *J Bone Miner Res.* 2004;19(4):652–660. <https://doi.org/10.1359/JBMR.0301254>
- Suva LJ, Hartman E, Dilley JD, et al. Platelet dysfunction and a high bone mass phenotype in a murine model of platelet-type von Willebrand disease. *Am J Pathol.* 2008;172(2):430–439. <https://doi.org/10.2353/ajpath.2008.070417>
- Giovacco WA, Goldberg CG, Taylor AF, et al. The role of gap junctions in megakaryocyte-mediated osteoblast proliferation and differentiation. *Bone.* 2009;44(1):80–86. <https://doi.org/10.1016/j.bone.2008.08.117>
- Olivos DJ 3rd, Alvarez M, Cheng YH, et al. Lnk deficiency leads to TPO-mediated osteoclastogenesis and increased bone mass phenotype. *J Cell Biochem.* 2017;118(8):2231–2240. <https://doi.org/10.1002/jcb.25874>
- Alvarez MB, Xu L, Childress PJ, et al. Megakaryocyte and osteoblast interactions modulate bone mass and hematopoiesis. *Stem Cells Dev.* 2018;27(10):671–682. <https://doi.org/10.1089/scd.2017.0178>
- Cwirla SE, Balasubramanian P, Duffin DJ, et al. Peptide agonist of the thrombopoietin receptor as potent as the natural cytokine. *Science.* 1997;276(5319):1696–1699. <https://doi.org/10.1126/science.276.5319.1696>
- Feese MD, Tamada T, Kato Y, et al. Structure of the receptor-binding domain of human thrombopoietin determined by complexation with a neutralizing antibody fragment. *Proc Natl Acad Sci USA.* 2004;101(7):1816–1821. <https://doi.org/10.1073/pnas.0308530100>
- Uhlén M, Fagerberg L, Hallström BM, et al. Proteomics. Tissue-based map of the human proteome. *Science.* 2015;347(6220):1260419. <https://doi.org/10.1126/science.1260419>
- Kuter DJ. The biology of thrombopoietin and thrombopoietin receptor agonists. *Int J Hematol.* 2013;98(1):10–23. <https://doi.org/10.1007/s12185-013-1382-0>
- Saleh MN, Bussel JB, Cheng G, et al. Safety and efficacy of eltrombopag for treatment of chronic immune thrombocytopenia: results of the long-term, open-label EXTEND study. *Blood.* 2013;121(3):537–545. <https://doi.org/10.1182/blood-2012-04-425512>
- Vishnu P, Aboulaflia DM. Long-term safety and efficacy of romiplostim for treatment of immune thrombocytopenia. *J Blood Med.* 2016;7:99–106. <https://doi.org/10.2147/JBM.S80646>
- Chu TM, Warden SJ, Turner CH, Stewart RL. Segmental bone regeneration using a load-bearing biodegradable carrier of bone morphogenetic protein-2. *Biomaterials.* 2007;28(3):459–467. <https://doi.org/10.1016/j.biomaterials.2006.09.004>
- Bhatti FUR, Dadwal UC, Valuch CR, et al. The effects of high fat diet, bone healing, and BMP-2 treatment on endothelial cell growth and function. *Bone.* 2021;146:115883. <https://doi.org/10.1016/j.bone.2021.115883>
- McKinley TO, Childress P, Jewell E, et al. Bone morphogenetic protein-2 rapidly heals two distinct critical sized segmental diaphyseal bone defects in a porcine model. *Mil Med.* 2023;188(1-2):117–124. <https://doi.org/10.1093/milmed/usab360>
- McKinley TO, Natoli RM, Fischer JP, et al. Internal fixation construct and defect size affect healing of a translational porcine diaphyseal tibial segmental bone defect. *Mil Med.* 2021;186(11-12):e1115–e1123. <https://doi.org/10.1093/milmed/usaa516>
- McKinley TO, Natoli RN, Janakiram NB, et al. Minced muscle autografting improves bone healing but not muscle function in a porcine composite injury model. *J Orthop Res.* 2023;41(9):1890–1901. <https://doi.org/10.1002/jor.25551>
- Low SA, Nielsen JJ, Coakley CM, et al. An engineered dual function peptide to repair fractured bones. *J Control Release.* 2022;350:688–697. <https://doi.org/10.1016/j.jconrel.2022.06.068>
- Whelan DB, Bhandari M, Stephen D, et al. Development of the radiographic union score for tibial fractures for the assessment of tibial fracture healing after intramedullary fixation. *J Trauma.* 2010;68(3):629–632. <https://doi.org/10.1097/TA.0b013e3181a7c16d>
- Chakraborty N, Muhie S, Kumar R, et al. Contributions of polyunsaturated fatty acids (PUFA) on cerebral neurobiology: an integrated omics approach with epigenomic focus. *J Nutr Biochem.* 2017;42:84–94. <https://doi.org/10.1016/j.jnutbio.2016.12.006>
- Hammamieh R, Muhie S, Borschel R, et al. Temporal progression of pneumonic plague in blood of nonhuman primate: a transcriptomic analysis. *PLoS One.* 2016;11(3):e0151788. <https://doi.org/10.1371/journal.pone.0151788>
- Hsiao YT, Manikowski KJ, Snyder S, et al. NMUR1 in the NMU-mediated regulation of bone remodeling. *Life (Basel).* 2021;11(10). <https://doi.org/10.3390/life11101028>
- Dadwal UC, Bhatti FUR, Awosanya OD, et al. The effects of bone morphogenetic protein 2 and thrombopoietin treatment on angiogenic properties of endothelial cells derived from the lung and bone marrow of young and aged, male and female mice. *FASEB J.* 2021;35(9):e21840. <https://doi.org/10.1096/fj.202001616RR>
- Dadwal UC, Bhatti FUR, Awosanya OD, et al. The effects of SRT1720 treatment on endothelial cells derived from the

- lung and bone marrow of young and aged, male and female mice. *Int J Mol Sci.* 2021;22:20. <https://doi.org/10.3390/ijms222011097>
33. Lieberman JR, Daluiski A, Stevenson S, et al. The effect of regional gene therapy with bone morphogenetic protein-2-producing bone-marrow cells on the repair of segmental femoral defects in rats. *J Bone Joint Surg Am.* 1999;81(7):905–917. <https://doi.org/10.2106/00004623-199907000-00002>
 34. Kantarjian H, Fenaux P, Sekeres MA, et al. Safety and efficacy of romiplostim in patients with lower-risk myelodysplastic syndrome and thrombocytopenia. *J Clin Oncol.* 2010;28(3):437–444. <https://doi.org/10.1200/JCO.2009.24.7999>
 35. Kimura T, Kaburaki H, Miyamoto S, Katayama J, Watanabe Y. Discovery of a novel thrombopoietin mimic agonist peptide. *J Biochem.* 1997;122(5):1046–1051. <https://doi.org/10.1093/oxfordjournals.jbchem.a021845>
 36. Case BC, Hauck ML, Yeager RL, et al. The pharmacokinetics and pharmacodynamics of GW395058, a peptide agonist of the thrombopoietin receptor, in the dog, a large-animal model of chemotherapy-induced thrombocytopenia. *Stem Cells.* 2000;18(5):360–365. <https://doi.org/10.1634/stemcells.18-5-360>
 37. Behrends DA, Khendek L, Gao C, Zayed N, Henderson JE, Martineau PA. Characterization of a pre-clinical mini-pig model of scaphoid non-union. *J Funct Biomater.* 2015;6(2):407–421. <https://doi.org/10.3390/jfb6020407>
 38. Kelada SN, Aylor DL, Peck BC, et al. Genetic analysis of hematological parameters in incipient lines of the collaborative cross. *G3 (Bethesda).* 2012;2(2):157–165. <https://doi.org/10.1534/g3.111.001776>
 39. Bouchard G, Liu J, Shoemak C, Brocksmith D, Trickey J, Teel A. *Miniature Swine Book of Normal Data (2017).* Sinclair BioResources, 2017.
 40. Devescovi V, Leonardi E, Ciapetti G, Cenni E. Growth factors in bone repair. *Chir Organi Mov.* 2008;92(3):161–168. <https://doi.org/10.1007/s12306-008-0064-1>
 41. Cardier JE, Dempsey J. Thrombopoietin and its receptor, c-mpl, are constitutively expressed by mouse liver endothelial cells: evidence of thrombopoietin as a growth factor for liver endothelial cells. *Blood.* 1998;91(3):923–929. <https://doi.org/10.1182/blood.V91.3.923>
 42. Yoder MC, Mead LE, Prater D, et al. Redefining endothelial progenitor cells via clonal analysis and hematopoietic stem/progenitor cell principals. *Blood.* 2007;109(5):1801–1809. <https://doi.org/10.1182/blood-2006-08-043471>
 43. Dadwal UC, Staut CA, Tewari NP, et al. Effects of diet, BMP-2 treatment, and femoral skeletal injury on endothelial cells derived from the ipsilateral and contralateral limbs. *J Orthop Res.* 2021;40(2):439–448. <https://doi.org/10.1002/jor.25033>
 44. Pearson HB, Mason DE, Kegelman CD, et al. Effects of bone morphogenetic protein-2 on neovascularization during large bone defect regeneration. *Tissue Eng Part A.* 2019;25(23-24):1623–1634. <https://doi.org/10.1089/ten.tea.2018.0326>
 45. Eguchi M, Masuda H, Kwon S, et al. Lesion-targeted thrombopoietin potentiates vasculogenesis by enhancing motility and enlivenment of transplanted endothelial progenitor cells via activation of Akt/mTOR/p70S6kinase signaling pathway. *J Mol Cell Cardiol.* 2008;45(5):661–669. <https://doi.org/10.1016/j.yjmcc.2008.08.002>
 46. Chandrasekhar KS, Zhou H, Zeng P, et al. Blood vessel wall-derived endothelial colony-forming cells enhance fracture repair and bone regeneration. *Calcif Tissue Int.* 2011;89(5):347–357. <https://doi.org/10.1007/s00223-011-9524-y>
 47. Kawakami Y, Ii M, Matsumoto T, et al. A small interfering RNA targeting Lnk accelerates bone fracture healing with early neovascularization. *Lab Invest.* 2013;93(9):1036–1053. <https://doi.org/10.1038/labinvest.2013.93>
 48. Kusumbe AP, Ramasamy SK, Adams RH. Coupling of angiogenesis and osteogenesis by a specific vessel subtype in bone. *Nature.* 2014;507(7492):323–328. <https://doi.org/10.1038/nature13145>
 49. Saul D, Khosla S. Fracture healing in the setting of endocrine diseases, aging, and cellular senescence. *Endocr Rev.* 2022;43(6):984–1002. <https://doi.org/10.1210/endrev/bnac008>
 50. Bethel M, Barnes CL, Taylor AF, et al. A novel role for thrombopoietin in regulating osteoclast development in humans and mice. *J Cell Physiol.* 2015;230(9):2142–2151. <https://doi.org/10.1002/jcp.24943>